Research Square

Preprints are preliminary reports that have not undergone peer review.
They should not be considered conclusive, used to inform clinical practice,
or referenced by the media as validated information.

Ozone concentration, not concentration-time dose, governs inactivation of dried human coronavirus on surfaces

Prawal P. K. Agarwal

prawal.agarwal@1-act.com

Advanced Cooling Technologies, Inc

Yong Mao

The State University of New Jersey

Karl S. Stevenson

Advanced Cooling Technologies, Inc

Petras Winkler

The State University of New Jersey

Aaron D. Mazzeo

The State University of New Jersey

Francois Berthiaume

The State University of New Jersey

Article

Keywords: ozone, surface decontamination, human coronavirus, disinfection kinetics, nonthermal plasma, CT value

Posted Date: November 12th, 2026

DOI: https://doi.org/10.21203/rs.3.rs-11462653/v1

License: This work is licensed under a Creative Commons Attribution 4.0 International License.
Read Full License

Additional Declarations: Competing interest reported. P.P.K.A. and K.S.S. are employees of Advanced Cooling Technologies, Inc., which developed the plasma reactor described in this work. The remaining authors declare no competing interests.

Abstract

Gaseous ozone reaches surfaces that liquid disinfectants and ultraviolet light cannot. Decontamination cycles are commonly specified by the concentration-time product CT, on the assumption that equal products give equal outcomes. We tested that assumption for human coronavirus 229E dried on polystyrene, using ozone generated from ambient air by a packed-electrode volumetric dielectric barrier discharge reactor. At the standard viral load, doubling the contact time raised the dose to 24,000 ppm·min and gave 2.8 $\log_{10}$, whereas raising the concentration from 200 to 250 ppm reached only 15,000 ppm·min yet gave 3.0 $\log_{10}$. With a fivefold larger inoculum the separation widened: 24,000 ppm·min at 200 ppm achieved 1.4 $\log_{10}$, while 15,000 ppm·min at 250 ppm achieved 2.3 $\log_{10}$. At both loads the larger integrated dose, delivered at the lower concentration, produced the smaller reduction. Exponents derived from the standard-load conditions are 1.2 for concentration and 0.3 for contact time, so concentration is roughly fourfold more influential. We attribute this to ozone diffusing into a dried organic film that consumes it. Across published surface studies the required CT spans more than three orders of magnitude. A cycle specified by CT alone can therefore under-decontaminate a surface while nominally meeting its dose target.

Introduction

Respiratory viruses deposited on surfaces remain a recognized route of transmission. Infectious severe acute respiratory syndrome coronavirus 2 (SARS-CoV-2) has been recovered from plastic and stainless steel for up to 72 h after deposition[1]; persistence is prolonged at lower temperatures[2]; and coronaviruses as a group survive on inanimate surfaces for periods ranging from hours to days[3]. Decontamination of high-touch surfaces is therefore a standard element of outbreak response, yet the methods in routine use are constrained in ways that limit their application to cluttered real interiors.

Liquid disinfectants must be applied to, and must wet, every surface that is to be treated. Vaporized hydrogen peroxide removes the wiping step and is effective against enveloped viruses[4,5], but requires a sealed enclosure, a dedicated generator and an aeration phase, and leaves condensate on cold surfaces. Ultraviolet germicidal irradiation is rapid and residue-free but acts only along the line of sight[6,7], so that recesses, undersides and the interiors of complex objects are shadowed. Both approaches scale poorly to the geometric complexity of occupied rooms.

Gaseous ozone addresses both constraints. Being a gas, it distributes by bulk flow and diffusion and so reaches shadowed and recessed surfaces that neither a wipe nor a photon can access[8,9]. It is generated electrically from ambient air on demand, so no oxidant need be stored. It also decomposes spontaneously to molecular oxygen, so no persistent film remains to be rinsed or neutralized. Its virucidal action on enveloped viruses proceeds by oxidation of the lipid envelope and of surface glycoproteins, progressively abolishing the ability to attach to and enter host cells[10–13].

Dielectric barrier discharge has made compact, air-fed ozone sources practical[14,15], and plasma-generated ozone has been applied to decontamination in several configurations. Forcing ozone through the fibers of filtering facepiece respirators shortened the required treatment time relative to a sealed enclosure[16]. Compact surface discharges have been used to inactivate bacteria in an open water system[17] and to decontaminate spacecraft materials, including penetration of woven fabrics[18], and a portable reactor has inactivated SARS-CoV-2 and a human coronavirus surrogate on porous and nonporous coupons[19]. Human coronavirus 229E (HCoV-229E), the strain used here, has itself been inactivated by plasma-generated ozone on glass[20] and on porous and nonporous materials[21]. In the present work ozone is supplied by a packed-electrode volumetric dielectric barrier discharge reactor operating on untreated ambient air (Fig. 1), whose design, discharge physics and energy performance are reported separately[22].

How such a treatment should be specified is a separate question, and one that has received much less scrutiny than efficacy. Disinfection practice inherits from water treatment the concentration-time product CT, the integral of disinfectant concentration over contact time, which follows from the Chick-Watson description of first-order inactivation by a disinfectant held at constant concentration[23–25]. Its transfer to gas-phase surface decontamination has been widespread: published surface studies and equipment specifications alike quote a CT target, which carries the implication that any combination of concentration and contact time giving the same product will give the same result. The assumption is seldom examined. It rests on conditions, namely a uniform disinfectant concentration that is not depleted by the target, that a dried organic deposit on a solid surface does not obviously satisfy.

Here we test that assumption directly. HCoV-229E, a surrogate for SARS-CoV-2 that can be handled at biosafety level 2[20,21], was dried on polystyrene and exposed to ozone generated from ambient air at two concentrations and two contact times, chosen so that the comparison isolates concentration at matched or larger integrated dose. We find that CT does not order the outcomes across viral loads, that the discrepancy widens as the organic burden of the deposit increases, and that the direction of the error is the one that matters for safety.

Results

Ozone delivery to the exposure chamber

The concentration presented to the samples was established before any biological exposure. At a fixed supply setting of 90 W, the outlet concentration fell monotonically with increasing airflow, from ~ 2,000 ppm under near-static conditions at 1 cubic foot per minute (CFM; 1 CFM = 28.3 L min^{-1}) to ~ 50 ppm at 75 CFM (Fig. 2a). Each concentration plotted was reproduced in three or more independent measurements. The decline reflects the shorter residence time in the discharge and the larger gas volume over which a fixed power is distributed. It is not uniform: the concentration falls by a further fourfold between 60 and 75 CFM, so the setpoint was held with an in-line flow meter. An airflow of 60

CFM (1.70 m^3 min^{-1}), which delivered ~ 200 ppm, was selected as the standard operating condition because it corresponds to a 5% slipstream of an air-handling unit of ~ 10.5 kW cooling capacity (nominally 3 tons), which circulates ~ 1,200 CFM.

Because the exposures lasted up to 120 min, the stability of the delivered concentration over that period was verified directly (Fig. 2b). At the 90 W setting the outlet concentration reached 200 ppm within the first few minutes and remained there for the full 240 min of observation and reproducibly across three or more runs, which covers both exposure windows with margin. The 250 ppm condition used in the inactivation experiments was obtained at the same 60 CFM airflow at a supply setting of ~ 120 W. Stability at that setting was not recorded directly and is inferred from the behavior at 90 W.

These measurements indicate that the 200 ppm exposure concentration was maintained for the duration of each treatment, so that the CT values quoted below for that condition are delivered rather than nominal doses. Supply settings are nominal and are not a measure of absorbed power, so no energy yield should be inferred from them; the energy performance of the reactor, its discharge physics and its thermal behavior are characterized in the companion study and are not reproduced here[22].

Inactivation of dried HCoV-229E

Infectivity was quantified by plaque assay at biosafety level 2 in a separate laboratory (Fig. 3). Relative to desiccation-matched controls, which were dried and handled identically but held in ozone-free air, a 60 min treatment at 200 ppm lowered the titer from 3.92 ± 0.13 to 1.60 ± 0.31 $\log_{10}$ PFU mL^{-1}, a reduction of 2.3 $\log_{10}$. Extending the exposure to 120 min at the same concentration gave 1.10 ± 0.32 $\log_{10}$ PFU mL^{-1}, a reduction of 2.8 $\log_{10}$, significantly below the 60 min value ($p < 0.005$; Fig. 3a). The controls confirmed that the losses were attributable to ozone rather than to drying.

Raising the concentration instead of the time was the more effective change. At a fixed 60 min exposure, increasing the concentration from 200 to 250 ppm lowered the titer to 0.91 ± 0.30 $\log_{10}$ PFU mL^{-1}, a reduction of 3.0 $\log_{10}$ and significantly below the 200 ppm value ($p < 0.05$; Fig. 3b). A 25% increase in concentration therefore achieved more inactivation, in half the time, than a doubling of contact time achieved.

Under a heavier contamination challenge the separation widened. In samples prepared with a fivefold larger inoculum volume (50 µL of stock rather than 10 µL), treatment at 200 ppm for 120 min lowered the titer from 4.87 ± 0.08 to 3.47 ± 0.10 $\log_{10}$ PFU mL^{-1}, a reduction of 1.4 $\log_{10}$, whereas treatment at 250 ppm for 60 min gave 2.55 ± 0.05 $\log_{10}$ PFU mL^{-1}, a reduction of 2.3 $\log_{10}$ ($p < 0.005$; Fig. 3c). The loss of efficacy at the higher burden does not follow from the higher starting titer as such, because a first-order process would give the same $\log_{10}$ reduction from any initial concentration. It is more consistent with a thicker, more ozone-consuming deposit left by the larger inoculum, a possibility considered in the Discussion.

Concentration and contact time are not interchangeable

Plotting the reductions against the integrated dose makes the failure of CT explicit (Fig. 4a). At the standard load, 200 ppm for 60 min delivered CT = 12,000 ppm·min and gave 2.3 $\log_{10}$. Doubling the contact time raised the dose to 24,000 ppm·min and the reduction to 2.8 $\log_{10}$. Increasing the concentration instead raised the dose only to 15,000 ppm·min, a quarter as much additional dose, yet gave a larger reduction of 3.0 $\log_{10}$. The smaller dose produced the greater inactivation.

The fivefold inoculum widened the same ordering. Treatment at 250 ppm for 60 min (CT = 15,000 ppm·min) gave 2.3 $\log_{10}$, whereas treatment at 200 ppm for 120 min, delivering a 60% larger CT of 24,000 ppm·min, gave only 1.4 $\log_{10}$. At both viral loads the larger integrated dose, delivered at the lower concentration, produced the smaller reduction, so CT does not order the outcomes.

The behavior is captured by a generalized rate expression in which the $\log_{10}$ reduction scales as $C^{*n*}t^{*m*}$, with n the dilution coefficient, a measure of how steeply inactivation responds to concentration[23–26]. The exponents implied by the three standard-load conditions are $n \approx 1.2$ and $m \approx 0.3$ (Fig. 4b), so that concentration is roughly fourfold more influential than contact time over the range examined: a 1.25-fold increase in concentration raised the reduction by 0.69 $\log_{10}$, whereas a 2.0-fold increase in exposure time raised it by only 0.50 $\log_{10}$. Because three conditions determine three parameters, this description retains no residual degrees of freedom and the exponents carry no uncertainty estimate; they should be read as a compact summary of the observed trend rather than as independently validated kinetic constants. They also do not transfer between viral loads: applied to the high-load series they would predict a smaller gap than the 0.9 $\log_{10}$ observed, so that the dominance of concentration is, if anything, stronger at the higher burden.

Comparison with published surface studies

Placing these results alongside published studies of ozone inactivation of coronaviruses on surfaces shows the same pattern at the level of the literature (Table 1). The integrated dose reported for broadly comparable $\log_{10}$ reductions spans more than three orders of magnitude, from 20 ppm·min on mask fabric[27] and 330 ppm·min for a reduction of at least 3.3 $\log_{10}$ on stainless steel[28] to the 15,000 to 24,000 ppm·min required here. A descriptor that varies this widely between studies reporting similar endpoints cannot be universal.

Table 1

Representative studies of ozone inactivation of coronaviruses on surfaces, compared with the present work. Entries were restricted to studies reporting an infectivity endpoint for a coronavirus deposited on a surface together with a stated gas-phase ozone concentration and exposure time, so that CT could be computed; studies reporting only nucleic acid detection, or reporting plasma treatment without a separately measured gas-phase concentration, were excluded. CT, concentration-time product; HCoV, human coronavirus; RH, relative humidity; n.r., not reported; n.m., not monitored; n.s., not statistically significant.

Study	Virus	Deposit and surface	O_3 (ppm)	Time	CT (ppm·min)	RH (%)	$\log_{10}$ reduction
Yano et al.[28]	SARS-CoV-2	Washed virus dried on stainless steel	1.0	60 min	60	60 to 80	1.5
Yano et al.[28]	SARS-CoV-2	Washed virus dried on stainless steel	6.0	55 min	330	60 to 80	≥ 3.3
Murata et al.[29]	SARS-CoV-2	Dried on stainless steel	0.1	10 h	60	~ 80	1.3
Murata et al.[29]	SARS-CoV-2	Dried on stainless steel	0.1	10 h	60	55	0.5 (n.s.)
Uppal et al.[33]	HCoV-OC43	Droplets on glass in serum-containing medium	25	10 min	250	45	3.0
Lee et al.[27]	HCoV-229E	Dried on KF94 mask fabric	120	10 s	20	n.r.	4.0
This work	HCoV-229E	Culture stock dried on polystyrene	250	60 min	15,000	n.m.	3.0
This work	HCoV-229E	Culture stock dried on polystyrene	200	120 min	24,000	n.m.	3.0

The spread is not random, and it tracks three variables that CT does not encode. Relative humidity is the clearest. Murata and co-workers found that an identical CT of 60 ppm·min gave a 1.3 $\log_{10}$ reduction at ~ 80% relative humidity but only 0.5 $\log_{10}$, not statistically significant, at 55%, a demonstration within a single study that equal CT need not give equal outcome[29]. The organic loading of the deposit is the second: the virus used by Yano and co-workers was ultrafiltered and washed before deposition, leaving very little proteinaceous soil[28], whereas the samples here were dried directly from culture stock and retain the full organic matrix. The third is the concentration at which the dose is delivered, which is the variable isolated in Fig. 4. The comparatively large CT required in the present work is consistent with its position on all three axes.

Discussion

The central observation of this study is that the integrated oxidative dose does not determine the outcome of ozone treatment of a virus dried on a solid surface, and that the concentration at which that dose is delivered is the stronger variable. The result holds at both viral loads examined, where the larger dose delivered at the lower concentration produced the smaller reduction, inverting the ordering that CT predicts.

A depletable-demand picture accounts for the asymmetry between the two exponents. A dried deposit of culture stock is not a clean monolayer of virions but a film of salts, proteins and medium components in which virions are embedded, and that organic matrix exerts a finite ozone demand which must be satisfied before the oxidant can advance. A higher external concentration satisfies that demand faster and so carries the reaction front deeper for a given integrated dose. Extending the time at a fixed concentration, by contrast, advances a diffusion-limited front only as the square root of time, so the returns diminish; the observed $m \approx 0.4$ is close to the value such a front would give. The same picture explains why the departure from CT widens with inoculum volume, since a larger deposit presents a larger demand. We note that a steady-state reaction-diffusion treatment with a non-depletable sink would predict a linear concentration dependence, so the concentration exponent exceeding unity is not established by these data alone; with three conditions and no uncertainty estimate, $n \approx 1.2$ is not distinguishable from unity. What the data do establish is the asymmetry between the two exponents, which is what the specification failure turns on. Sub-linear returns in time are also the signature of tailing, consistent with a subpopulation of virions shielded within the matrix, a behavior long recognized in disinfection kinetics[23–26] but usually treated as a deviation from the model rather than as a reason to question the dose descriptor itself.

The practical consequence is a specification failure, and it runs in the unsafe direction. A practitioner who validates a cycle at one concentration and then reproduces the same CT at a lower concentration over a longer time, which is the natural response to an occupancy or ventilation constraint, obtained less inactivation than the validated cycle delivered in both series examined here, while the instrumentation would report that the dose target had been met. At the standard load that substitution cost 0.2 $\log_{10}$ despite a 60% larger nominal dose, and at the fivefold inoculum it cost 0.9 $\log_{10}$. A decontamination specification for a dried surface should therefore state the concentration at which the dose was validated, and a cycle should not be re-derived at a different concentration without revalidation. Concentration intensification, where the apparatus permits it, is also the more efficient route to a target reduction.

Several limitations bound these conclusions. Infectivity was measured on a single substrate, polystyrene, so the generality of the quantitative exponents across surface chemistries and roughnesses is untested, although the mechanism invoked depends on the deposit rather than on the substrate. The comparisons on which the central claim rests were tested directly between treated conditions and were significant at both loads, but each rests on three replicates, so the exponents derived from them remain indicative rather than precise. Relative humidity was not monitored during the exposures, which were performed in unconditioned ambient air. Since the hydroxyl-radical pathway that contributes to ozone virucidal activity

is enhanced at high humidity[29,30], humidification is a clear route to lowering the required CT and a priority for optimization, and the unmonitored humidity is the most likely single reason the doses here exceed those of humidified studies. The treated titers at the standard load lie within an order of magnitude of the quantification limit of the plaque assay, which compresses the differences between them. Nitrogen oxides and the oxygenated byproducts formed when ozone reacts with surface organics were not quantified, so the residue-free character of the method refers to the absence of a persistent disinfectant film rather than to the absence of reaction products. Finally, the working concentrations of 200 to 250 ppm exceed occupational exposure limits by more than three orders of magnitude[31], and all exposures were accordingly confined to a containment loop whose effluent passed through a catalytic destructor that returned residual ozone to molecular oxygen before venting[32]; the hazard controls are set out in the Methods.

Within those bounds, the finding is robust and transferable. Gaseous ozone inactivates a dried human coronavirus on a solid surface, and the rate at which it does so is governed more strongly by concentration than by the integrated concentration-time dose. Dose alone is an incomplete specification for surface decontamination, and reporting it without the concentration at which it was delivered discards the variable that matters most.

Methods

Decontamination system

Ozone was generated by a packed-electrode volumetric dielectric barrier discharge reactor comprising 97 type 316L stainless steel rod electrodes of 3 mm diameter, each sheathed in a fused-quartz tube of 4 mm outer diameter. The sheaths are packed in mutual contact on a hexagonal lattice of 4.0 mm pitch within a quartz housing of 52 mm inner diameter, the electrode bundle being 305 mm (12 in) long. High-voltage and grounded rods alternate by row, forming a three-dimensional network of sub-millimeter interstitial voids in which the discharge is sustained. The reactor was driven by a custom alternating-current high-voltage supply. Its design, discharge physics, electrical characterization and energy performance are reported separately[22] and were not re-measured here; supply settings are quoted throughout as nominal values and are not a measure of absorbed power.

For the present experiments the reactor was integrated into a bench-scale decontamination system configured to emulate a 5% slipstream of an air-handling unit of ~ 10.5 kW cooling capacity, nominally 3 tons (Fig. 1). Ambient air was drawn by a variable-speed blower through an in-line flow meter and the reactor, and the ozone-laden stream passed through a connecting duct into a gas-tight 1 ft^3 (28.3 L) acrylic exposure chamber holding the samples. The chamber effluent was returned through a catalytic ozone destructor before venting.

Ozone generation and measurement

Ozone concentration was measured by ultraviolet absorption at 254 nm with a UV-106-MH analyzer (2B Technologies), sampling the effluent through a T-connection at the reactor outlet. The instrument covers 0 to 10,000 ppm with a resolution of 0.1 ppm and a stated accuracy of 0.05 ppm or 2% of reading. The dependence of concentration on volumetric airflow was characterized from 1 to 75 CFM at a fixed 90 W supply setting, and the stability of the delivered concentration was recorded for 240 min at the 90 W setting and a constant 60 CFM. Each reported concentration was recorded in three or more independent measurements, and repeat readings returned the same value at the precision reported here, so no error bars are shown in Fig. 2. The 200 ppm exposure condition corresponds to the 90 W setting at 60 CFM; the 250 ppm condition was obtained at the same airflow at a setting of ~ 120 W. Airflow, chamber geometry, sample preparation and exposure protocol were identical between the two conditions.

Virus and cells

HCoV-229E was used as a biosafety level 2 surrogate for SARS-CoV-2. Virus was propagated and titrated in MRC-5 human lung fibroblasts maintained in MEM-alpha supplemented with 10% fetal bovine serum and 25 µg mL^{-1} gentamicin; assay medium was the same base with 2% fetal bovine serum. Cells were used between passages 16 and 20. The working stock was prepared at a titer of 2.6×10^6 PFU mL^{-1} and stored at -80°C until use. Virus was not washed or ultrafiltered before deposition, so the dried deposits retain the full organic burden of the culture medium.

Surface viral inactivation

Aliquots of viral stock, either 10 µL (standard load) or 50 µL (fivefold larger inoculum volume), were spread onto sterile 35 mm polystyrene surfaces and air-dried in a biosafety cabinet for 10 to 30 min to simulate dried fomite contamination. Dried samples were transferred to the exposure chamber and treated under one of three conditions: 200 ppm for 60 min, 200 ppm for 120 min, or 250 ppm for 60 min. The fivefold-inoculum samples were treated at 200 ppm for 120 min or at 250 ppm for 60 min. Desiccation-matched control samples were prepared and handled identically but held in ozone-free air for the same interval, so that the reported reductions are attributable to ozone rather than to drying. After each treatment the discharge was switched off and the chamber purged with ozone-free air for a further 2 min before the samples were removed. All exposures were performed in triplicate.

Plaque assay

Each treated or control sample was rehydrated in 250 µL of assay medium by pipetting, and serial tenfold dilutions were prepared in the same medium. Volumes of 200 µL were inoculated onto 90% confluent MRC-5 monolayers in six-well plates and adsorbed for 90 min at 37°C, with rocking every 20 min. The inoculum was then removed and each well overlaid with 2 mL of MEM-alpha containing 2% fetal bovine serum and 1% carboxymethylcellulose. Plates were incubated at 37°C in 5% CO_2; plaques

were imaged and counted on day 4 and confirmed by crystal violet staining on day 6, the two counts being comparable. Titers are reported as PFU mL^{-1}, and $\log_{10}$ reductions were computed relative to the desiccation-matched control processed in the same experiment.

Concentration-time analysis and statistics

The integrated oxidative dose for each condition was computed as the CT value. Because the ozone concentration was constant over the exposure at the 90 W setting (Fig. 2b), the integral of concentration over time reduces to the product of concentration (ppm) and exposure time (min). One feature of the exposure configuration bears on the interpretation of these values: the chamber was operated as a continuously purged flow-through volume rather than as a sealed batch. At 60 CFM the 1 ft^3 chamber is exchanged ~once per second, corresponding to more than 3,000 air changes during a 60 min exposure, so that ozone consumed at surfaces or lost to self-decomposition was continuously replenished and the chamber concentration tracks the reactor outlet rather than decaying from an initial charge.

Dose-response behavior was described using a generalized rate expression in which the $\log_{10}$ reduction scales as $C^{*n*}t^{*m*}$, with n the dilution coefficient and m the time exponent[23–26]. The two exponents and the proportionality constant were determined from the three standard-load conditions; because three observations determine three parameters, the description has no residual degrees of freedom, no goodness of fit is quoted, and the exponents carry no uncertainty estimate. Titers are reported as the mean ± standard deviation of triplicate measurements (n = 3). The two treated conditions within each panel of Fig. 3 were compared with one another by two-tailed Student's t-test; $p < 0.05$ was considered significant and is denoted by a single asterisk, with $p < 0.005$ denoted by three asterisks.

Hazard controls

Ozone is the hazard governing the safe conduct of this work, and the controls applied are reported so that the protocol can be reproduced safely. The Occupational Safety and Health Administration permissible exposure limit is 0.1 ppm as an 8 h time-weighted average, and the National Institute for Occupational Safety and Health value for conditions immediately dangerous to life or health is 5 ppm[31]. The 200 to 250 ppm working concentrations are therefore more than three orders of magnitude above the permissible exposure limit, and no exposure of personnel to the working atmosphere is permissible at any point in the procedure.

Two features of the method limit the hazard at source. Ozone is generated electrically from ambient air on demand, so no oxidant is stored or transported and production ceases within seconds of the discharge being de-energized. Ozone also decomposes spontaneously to molecular oxygen, so treated surfaces require no rinsing or chemical neutralization. The principal engineering control is destruction of the ozone before it can leave the system: the reactor and chamber form a containment loop whose

entire effluent passes through a catalytic destructor that converts residual ozone back to molecular oxygen before venting[32]. Because the loop is purged continuously at 60 CFM, clearance after the discharge is switched off is governed by the throughput of the destructor rather than by the slower natural decay of ozone. The assembly was operated within a certified fume hood, which provides secondary containment.

Administrative controls completed the sequence. A written standard operating procedure required the discharge to be de-energized and the chamber purged for a defined interval before any sample was retrieved, restricted access while the discharge was energized, and specified the personal protective equipment to be worn. Ozone concentration was followed by ultraviolet photometry throughout, so clearance before access was confirmed by measurement rather than inferred from elapsed time. Two residual risks are not closed by these controls and are discussed above: the oxidation byproducts were not quantified, and the conversion efficiency and service life of the destructor were not characterized.

Declarations

Competing Interests

P.P.K.A. and K.S.S. are employees of Advanced Cooling Technologies, Inc., which developed the plasma reactor described in this work. The remaining authors declare no competing interests.

Author Contribution

P.P.K.A. conceived the study, designed the reactor and decontamination system, performed the ozone generation and delivery experiments, analyzed the data and wrote the manuscript. Y.M. performed the virological experiments and plaque assays. K.S.S. contributed to reactor fabrication and electrical characterization. P.W. contributed to the exposure experiments. A.D.M. and F.B. supervised the biological testing and contributed to interpretation. All authors reviewed and approved the manuscript.

Acknowledgement

This work was supported by the U.S. Department of Energy under Small Business Innovation Research Phase I contract DE-SC0025766. The authors thank Devon Jensen of Advanced Cooling Technologies, Inc. for continued support. The views and opinions expressed herein are those of the authors and do not necessarily reflect those of the U.S. Department of Energy.

Data Availability

All data generated or analysed during this study are included in this published article, in its figures and in Table 1.

References

1. van Doremalen, N. et al. Aerosol and surface stability of SARS-CoV-2 as compared with SARS-CoV-1. *N Engl. J. Med.* **382**, 1564–1567 (2020).
2. Riddell, S., Goldie, S., Hill, A., Eagles, D. & Drew, T. W. The effect of temperature on persistence of SARS-CoV-2 on common surfaces. *Virol. J.* **17**, 145 (2020).
3. Kampf, G., Todt, D., Pfaender, S. & Steinmann, E. Persistence of coronaviruses on inanimate surfaces and their inactivation with biocidal agents. *J. Hosp. Infect.* **104**, 246–251 (2020).
4. Goyal, S. M., Chander, Y., Yezli, S. & Otter, J. A. Evaluating the virucidal efficacy of hydrogen peroxide vapour. *J. Hosp. Infect.* **86**, 255–259 (2014).
5. McEvoy, B. & Rowan, N. J. Terminal sterilization of medical devices using vaporized hydrogen peroxide: a review of current methods and emerging opportunities. *J. Appl. Microbiol.* **127**, 1403–1420 (2019).
6. Heßling, M., Hönes, K., Vatter, P. & Lingenfelder, C. Ultraviolet irradiation doses for coronavirus inactivation: review and analysis of coronavirus photoinactivation studies. *GMS Hyg. Infect. Control*. **15**, Doc08 (2020).
7. Criscuolo, E. et al. Fast inactivation of SARS-CoV-2 by UV-C and ozone exposure on different materials. *Emerg. Microbes Infect.* **10**, 206–209 (2021).
8. Epelle, E. I. et al. Ozone application in different industries: a review of recent developments. *Chem. Eng. J.* **454**, 140188 (2023).
9. Kim, J. G., Yousef, A. E. & Dave, S. Application of ozone for enhancing the microbiological safety and quality of foods: a review. *J. Food Prot.* **62**, 1071–1087 (1999).
10. Roy, D., Wong, P. K. Y., Engelbrecht, R. S. & Chian, E. S. K. Mechanism of enteroviral inactivation by ozone. *Appl. Environ. Microbiol.* **41**, 718–723 (1981).
11. Murray, B. K. et al. Virion disruption by ozone-mediated reactive oxygen species. *J. Virol. Methods*. **153**, 74–77 (2008).
12. Bayarri, B., Cruz-Alcalde, A., López-Vinent, N., Micó, M. M. & Sans, C. Can ozone inactivate SARS-CoV-2? A review of mechanisms and performance on viruses. *J. Hazard. Mater.* **415**, 125658 (2021).
13. Bae, J. et al. Mechanisms of plasma ozone and UV-C sterilization of SARS-CoV-2 explored through atomic force microscopy. *ACS Appl. Mater. Interfaces*. **16**, 49176–49185 (2024).
14. Kogelschatz, U. Dielectric-barrier discharges: their history, discharge physics, and industrial applications. *Plasma Chem. Plasma Process.* **23**, 1–46 (2003).
15. Lu, X. et al. Reactive species in non-equilibrium atmospheric-pressure plasmas: generation, transport, and biological effects. *Phys. Rep.* **630**, 1–84 (2016).

16. Schwan, J. et al. Efficient facemask decontamination via forced ozone convection. *Sci. Rep.* **11**, 12263 (2021).
17. Choudhury, B. et al. Inactivation of *Pseudomonas aeruginosa* and methicillin-resistant *Staphylococcus aureus* in an open water system with ozone generated by a compact, atmospheric DBD plasma reactor. *Sci. Rep.* **8**, 17573 (2018).
18. Choudhury, B. et al. Distributed compact plasma reactor decontamination for planetary protection in space missions. *Sci. Rep.* **13**, 1928 (2023).
19. Choudhury, B., Lednicky, J., Loeb, J. C., Portugal, S. & Roy, S. Inactivation of SARS-CoV-2 on porous and nonporous surfaces by compact portable plasma reactor. *Front. Bioeng. Biotechnol.* **12**, 1325336 (2024).
20. Bhartiya, P. et al. Nonthermal plasma-generated ozone inhibits human coronavirus 229E infectivity on glass surface. *Plasma Process. Polym.* **19**, e2200054 (2022).
21. Ashokkumar, S. et al. Human coronavirus 229E inactivation on porous and nonporous materials using dielectric barrier discharge (DBD) plasma. *J. Med. Virol.* **96**, e29655 (2024).
22. Agarwal, P. P. K. & Stevenson, K. S. Packed electrode volumetric dielectric barrier discharge (PEVDBD) plasma reactor: design, physics, and multi-application performance. *Preprint at.* https://doi.org/10.2139/ssrn.7222598 (2026).
23. Chick, H. An investigation of the laws of disinfection. *J. Hyg.* **8**, 92–158 (1908).
24. Watson, H. E. A note on the variation of the rate of disinfection with change in the concentration of the disinfectant. *J. Hyg.* **8**, 536–542 (1908).
25. Hunt, N. K. & Mariñas, B. J. Inactivation of *Escherichia coli* with ozone: chemical and inactivation kinetics. *Water Res.* **33**, 2633–2641 (1999).
26. Hom, L. W. Kinetics of chlorine disinfection in an ecosystem. *J. Sanit. Eng. Div.* **98**, 183–194 (1972).
27. Lee, J. et al. Fast and easy disinfection of coronavirus-contaminated face masks using ozone gas produced by a dielectric barrier discharge plasma generator. *Environ. Sci. Technol. Lett.* **8**, 339–344 (2021).
28. Yano, H. et al. Inactivation of severe acute respiratory syndrome coronavirus 2 (SARS-CoV-2) by gaseous ozone treatment. *J. Hosp. Infect.* **106**, 837–838 (2020).
29. Murata, T. et al. Reduction of severe acute respiratory syndrome coronavirus 2 infectivity by admissible concentration of ozone gas and water. *Microbiol. Immunol.* **65**, 10–16 (2021).
30. Farooq, S. & Tizaoui, C. A critical review on the inactivation of surface and airborne SARS-CoV-2 virus by ozone gas. *Crit. Rev. Environ. Sci. Technol.* **53**, 87–109 (2023).
31. Nuvolone, D., Petri, D. & Voller, F. The effects of ozone on human health. *Environ. Sci. Pollut Res.* **25**, 8074–8088 (2018).
32. Namdari, M., Lee, C. S. & Haghighat, F. Active ozone removal technologies for a safe indoor environment: a comprehensive review. *Build. Environ.* **187**, 107370 (2021).

33. Uppal, T., Khazaieli, A., Snijders, A. M. & Verma, S. C. Inactivation of human coronavirus by FATHHOME's dry sanitizer device: rapid and eco-friendly ozone-based disinfection of SARS-CoV-2. *Pathogens* 10, 339 (2021).

Figures

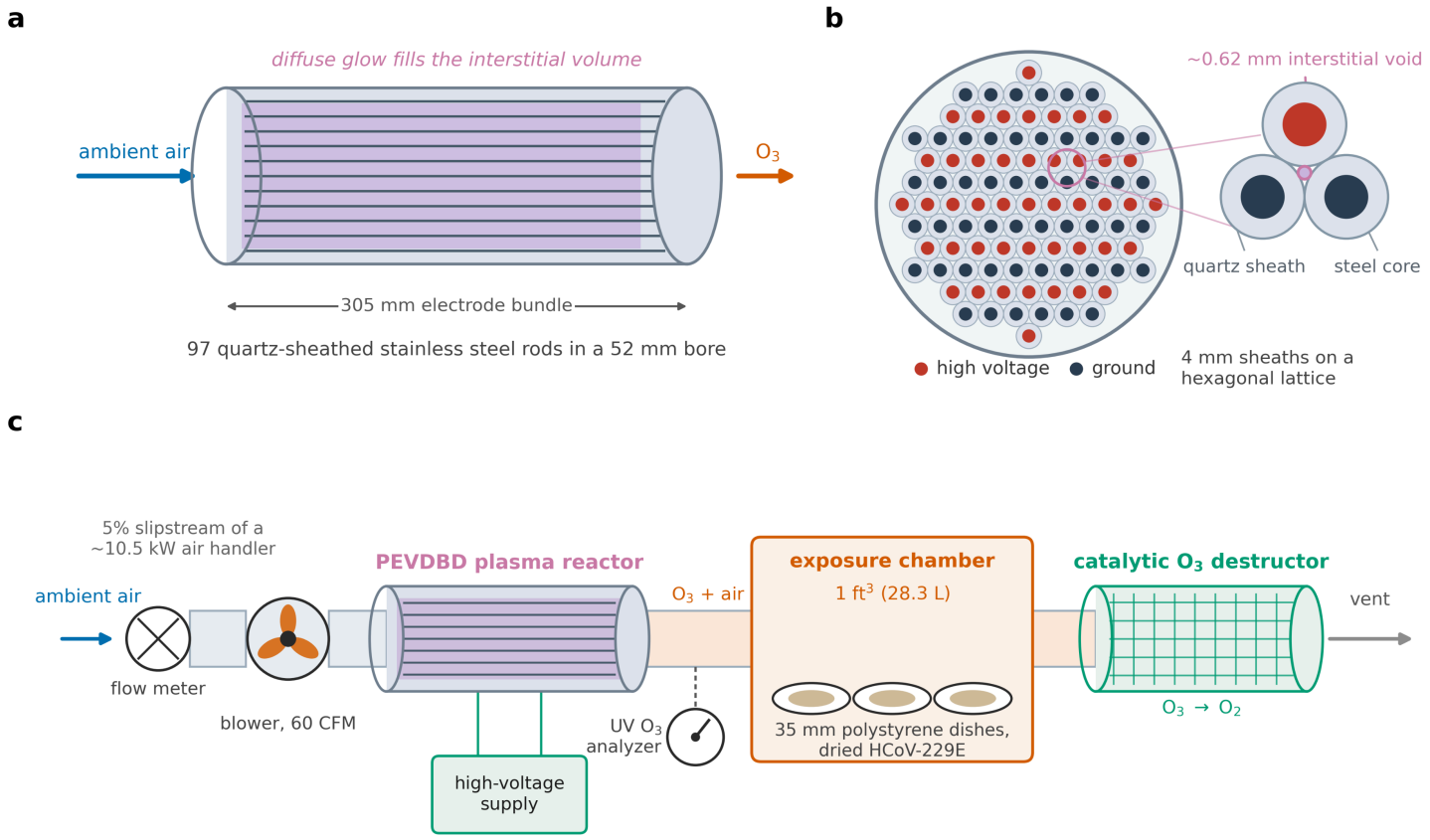


Figure 1

The packed-electrode reactor and the decontamination system. (**a**) Cutaway of the reactor: ambient air entering the packed array of quartz-sheathed rod electrodes is converted to ozone within a diffuse, atmospheric-pressure glow that fills the interstitial volume. (**b**) Cross-section of the electrode array. Ninety-seven quartz-sheathed rods are packed in mutual contact on a hexagonal lattice of 4.0 mm pitch within a 52 mm bore, with high-voltage and grounded rods alternating by row; the circled feature marks one of the triangular interstitial voids of ~0.62 mm inscribed diameter in which the discharge is sustained. (**c**) The decontamination system, configured as a 5% slipstream of an air-handling unit of ~10.5 kW cooling capacity. Ambient air is drawn through an in-line flow meter and the reactor, and the ozone-laden stream passes into a gas-tight 1 ft^3 (28.3 L) chamber holding 35 mm polystyrene dishes carrying dried human coronavirus 229E (HCoV-229E). Ozone is measured by ultraviolet photometry on a sample stream drawn at the reactor outlet, and the chamber effluent passes through a catalytic

destructor that returns residual ozone to molecular oxygen before venting. Panels are schematic and not to scale; the reactor design is reported separately[22].

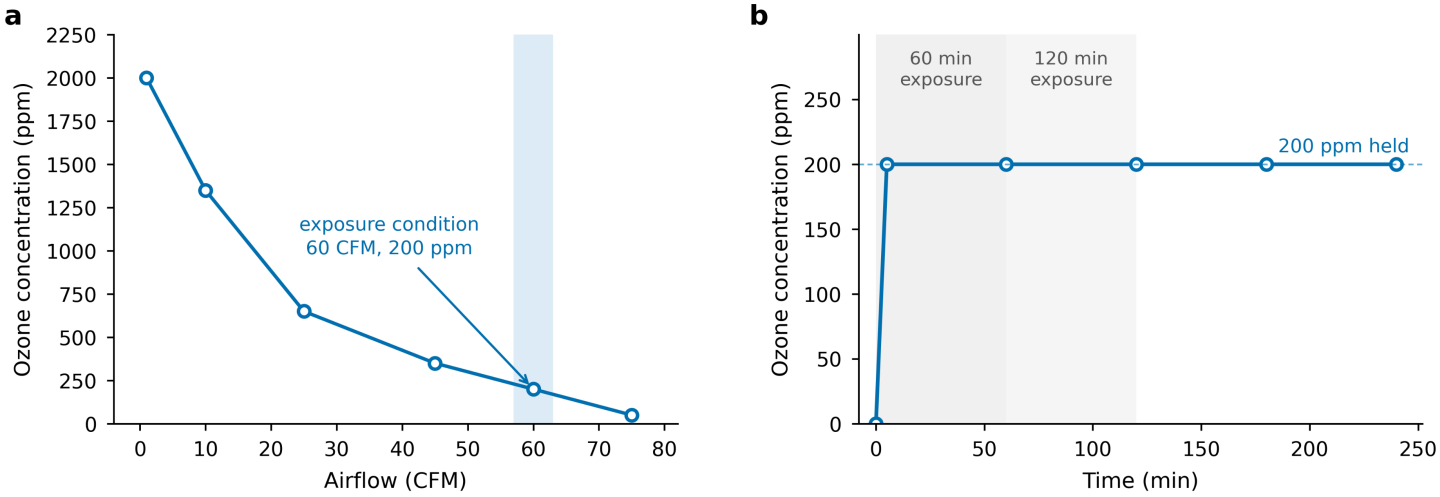


Figure 2

Ozone delivery to the exposure chamber. (**a**) Outlet ozone concentration versus airflow at a fixed 90 W supply setting, in cubic feet per minute (CFM; 1 CFM = 28.3 L min^{-1}). The concentration falls monotonically from ~2,000 ppm at 1 CFM to ~50 ppm at 75 CFM. The shaded band marks the 60 CFM operating condition used for all exposures. Each point was recorded in three or more independent measurements, which returned the same concentration, so the scatter is smaller than the plotted symbols. (**b**) Outlet ozone concentration versus time at the 90 W setting and a constant 60 CFM, the condition used for the 200 ppm exposures. The concentration reaches 200 ppm within the first few minutes and is held for the full 240 min of observation; the shaded bars mark the 60 min and 120 min exposure windows. The trace was reproduced in three or more independent runs.

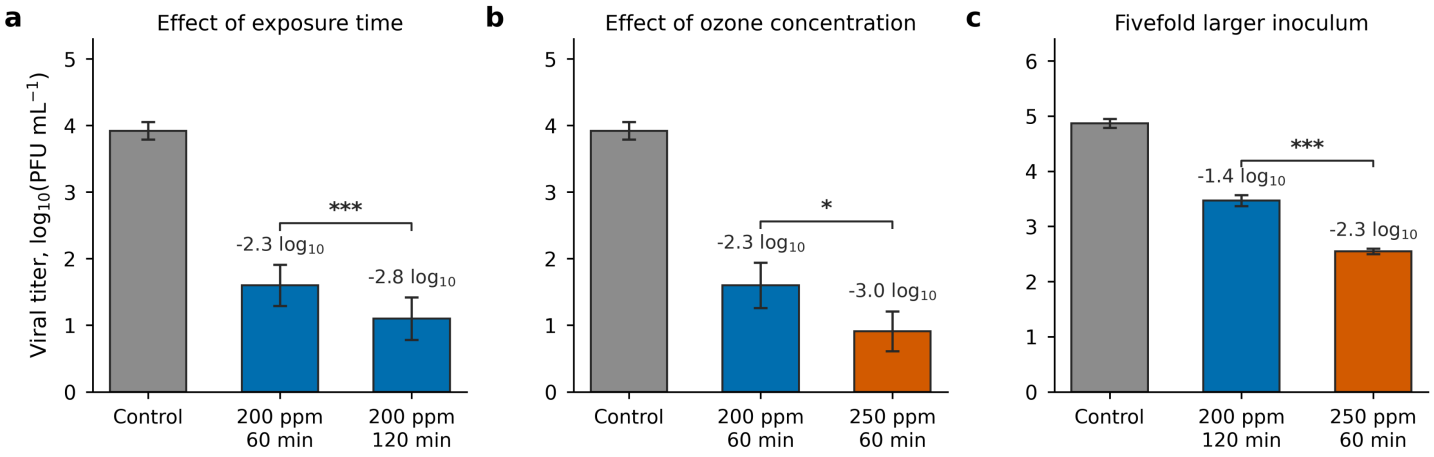


Figure 3

Inactivation of dried HCoV-229E, quantified by plaque assay. (**a**) Effect of exposure time at 200 ppm. (**b**) Effect of ozone concentration at a fixed 60 min exposure. (**c**) Fivefold larger inoculum volume (50 µL of stock rather than 10 µL). Bars are means and error bars standard deviations of *n* = 3 replicates per condition; the plotted quantity is the base-10 logarithm of the infectious titer in plaque-forming units per milliliter (PFU mL^{-1}). Values above each treated bar give the $\log_{10}$ reduction relative to the desiccation-matched control, which was dried and handled identically but held in ozone-free air. Brackets compare the two treated conditions with one another by two-tailed Student's *t*-test: *$p < 0.05$; ***$p < 0.005$.

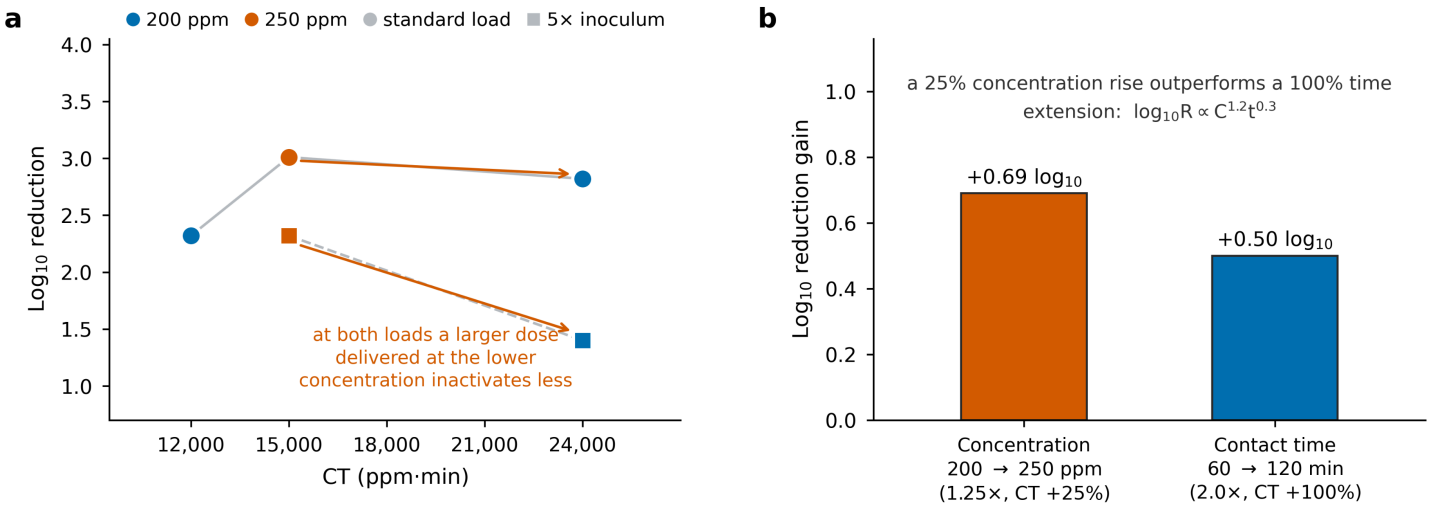


Figure 4

Concentration and contact time at matched concentration-time dose. (**a**) Log_{10} reduction versus CT, the product of ozone concentration and exposure time. Marker color denotes ozone concentration (200 ppm, blue; 250 ppm, vermillion) and marker shape denotes viral load (circles, 10 µL standard load; squares, 50 µL fivefold inoculum). Points at matched or larger CT that differ in reduction identify the failure of CT as a descriptor. (**b**) Increase in $\log_{10}$ reduction relative to the 200 ppm, 60 min condition, for a 1.25-fold increase in concentration and a 2.0-fold increase in contact time. The exponents *n* and *m* are those of the generalized rate expression in which $\log_{10}$ reduction scales as $C^{*n*}t^{*m*}$; the values shown follow from the three standard-load conditions and carry no uncertainty estimate, since three observations determine three parameters. Points are means of n = 3 replicates.